DOI: 10.1002/ejic.200800249

Complexes of Yb^{3+} with EDTA and CDTA – Molecular and Electronic Structure

Rafał Janicki,[a] Przemysław Starynowicz,[a] and Anna Mondry*[a]

Keywords: X-ray diffraction / Absorption / Density functional calculations / N,O ligands / Ytterbium

Two Yb^{3+} compounds, $[C(NH_2)_3]_2[Yb(EDTA)(H_2O)_2]ClO_4 \cdot 6H_2O$ and $[C(NH_2)_3][Yb(CDTA)(H_2O)_2] \cdot 4H_2O$, where EDTA is the ethylenediaminetetraacetate anion and CDTA is the *trans*-1,2-diaminecyclohexane-*N*,*N*,*N*′,*N*′-tetraacetate anion, were obtained and their crystal structures and spectroscopic properties were determined. In both compounds, the coordination geometries of the eight-coordinate Yb^{3+} ion are very similar. In each case, the inner sphere of the metal ion consists of four carboxyl oxygen atoms, two nitrogen atoms and two water molecules. The complexes were characterized by UV/Vis/NIR absorption at different temperatures and IR spectroscopy. The spectroscopic results revealed high sensitivity of the electronic $4f^{13}$ configuration upon minor changes in the coordination geometry around the Yb^{3+} ion. These data also demonstrate that species present in solutions of Yb^{3+}–EDTA are similar to those found in the crystal, whereas in solutions of Yb^{3+}–CDTA an equilibrium between at least two different forms exists. For the Yb^{3+}–EDTA complex in solution and in the crystalline state, a charge-transfer transition was detected. Theoretical calculations revealed its complicated (Yb → ligand and ligand → Yb) character.

Introduction

Lanthanide polyaminopolycarboxylates have been extensively studied for many years, as they have found a variety of applications, particularly in biochemical investigations and medicine. Owing to their high thermodynamic stability,[1] they are used as contrast agents in MRI imaging,[2] luminescent tags in immunoassays[3] as well as shift reagents of important physiological metal ions in NMR spectroscopy.[4] Recently, remarkable interest has been focused on lanthanide complexes that emit in the near-infrared (NIR) spectral region, and particularly, Nd^{3+} and Yb^{3+} compounds, because of their possible role as NIR emitters in medical diagnostics.[5] Although the luminescence of Nd^{3+} may be augmented by energy transfer from ligand states to the higher excited $4f^3$ levels of the metal cation, sensitized luminescence from the Yb^{3+} ion through the charge-transfer (CT) state also plays an important role.[6]

In the electronic spectra of the Yb^{3+} ion, the only f–f transition ($^2F_{7/2} \leftrightarrow {}^2F_{5/2}$) occurs at around 980 nm. This transition, which obeys the selection rules $\Delta J = 1$, $\Delta L = 0$, $\Delta S = 0$, has a mixed electric- and magnetic-dipole character, and its intensity is moderately dependent on the ytterbium ion environment.[7] Nevertheless, the crystal-field splittings of the $^2F_{7/2}$ and $^2F_{5/2}$ levels may provide useful information regarding investigated Yb^{3+} entities. As knowledge of physicooptical properties of ytterbium polyaminopolycarboxylates is still fragmentary, we decided to obtain crystalline compounds of Yb^{3+} with EDTA and CDTA as good model complexes for studying the influence of ligand modification on the $^2F_{7/2} \rightarrow {}^2F_{5/2}$ transition. In addition, we sought to learn by experimental and theoretical methods the nature of the CT transition in these compounds. Combination of the results from electronic spectroscopy and X-ray diffraction may be applied to interpret the physicochemical properties of species existing in solutions, as it was demonstrated previously for lanthanide polyaminopolycarboxylates[8] and polyaminopolyphosphonates.[9] We have therefore performed a comparison between the spectra of Yb^{3+}–EDTA and Yb^{3+}–CDTA complexes obtained in the form of crystals and in solutions to find the similarities and differences between the coordination behaviour of the two ligands towards the Yb^{3+} ion in both phases.

Results and Discussion

Crystal Structures

The crystal structures of $[C(NH_2)_3]_2[Yb(EDTA)(H_2O)_2]ClO_4 \cdot 6H_2O$ (crystal **1**) and $[C(NH_2)_3][Yb(CDTA)(H_2O)_2] \cdot 4H_2O$ (crystal **2**) were determined. Both crystals are composed of monomeric anions $[Yb(EDTA)(H_2O)_2]^-$ or $[Yb(CDTA)(H_2O)_2]^-$, respectively, guanidinium cations, water molecules, and in the case of Yb^{3+}–EDTA also of perchlorate anions. It is worth noting that although almost all lanthanide(III) complexes with ethylenediaminetetraacetic acid are monomeric,[9b,10] the known crystal structures

[a] Faculty of Chemistry, University of Wrocław,
F. Joliot-Curie 14, 50-383 Wrocław, Poland
Fax: +048-71-328-23-48
E-mail: anm@wchuwr.pl

of light lanthanide complexes with the cyclohexyldiaminetetraacetate ligand tend to form polymeric forms.[11,12] The metal cations in the present structures adopt similar coordination patterns in both structures, that is, all are eight-coordinate, and their first coordination spheres are composed of four carboxylate oxygen atoms, two nitrogen atoms and two water molecules each. Views of the complex anions are presented in Figures 1 and 2.

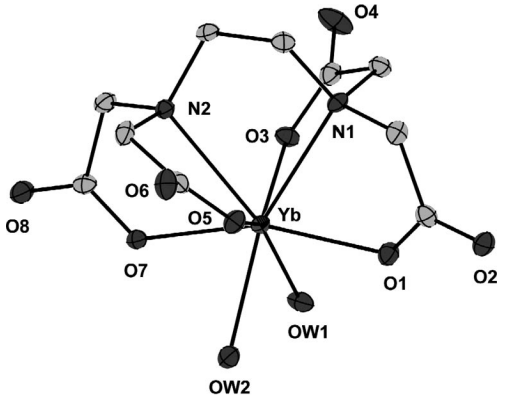

Figure 1. Molecular structure of the $[Yb(EDTA)(H_2O)_2]^-$ anion together with the atom numbering scheme.

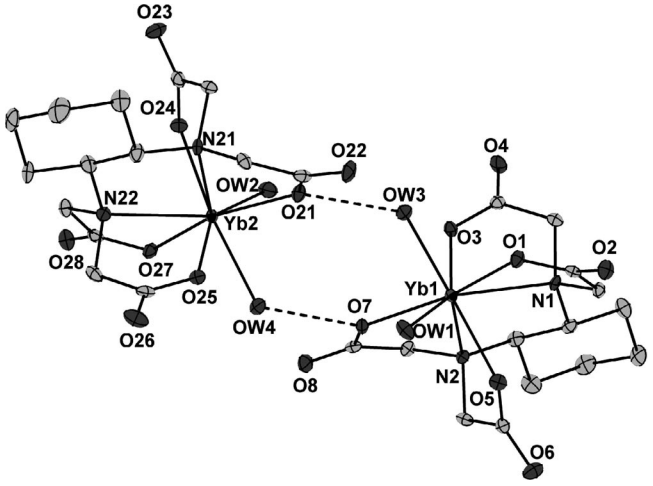

Figure 2. Molecular structure of the $[Yb(CDTA)(H_2O)_2]^-$ anions together with the atom numbering scheme; hydrogen bonds are rendered by dashed lines.

The Yb–O and Yb–N distances (Table 1) are similar, although those involving carboxylate oxygen atoms are slightly shorter in the case of the EDTA complex [average 2.254(25) Å] than those in the CDTA compound [average 2.270(12) Å]. The reverse tendency may be observed for the Yb–N bonds: the average is 2.577(7) Å for the EDTA complex and 2.549(10) Å for the CDTA one. The average Yb–O(water) separations are almost similar: 2.322(2) and 2.317(22) Å for EDTA and CDTA complexes, respectively. The carboxylate C–O bonds are longer when the O atoms are coordinated to Yb [the respective averages are 1.279(5) and 1.281(7) Å for EDTA and CDTA] than in the case of uncoordinated O atoms [EDTA 1.236(6) Å, CDTA 1.240(2) Å]. Both structures possess their particular individual features. In the structure of **1**, the symmetry-independent perchlorate anion is located closely to an inversion centre, namely, the distance between the perchlorate O14 atoms and its symmetry-generated offspring is 2.818(4) Å, which suggests the presence of a hydrogen bond. The positive charge of the presumed hydrogen cation must be compensated by an anion. As no additional discernible anions occur in the structure, the negative charge must come from abstraction of H^+ from a water molecule. Analysis of the water–water distances and the network of the hydrogen bonds reveals that this may be the case for OW7 and/or OW8, which form H–bonded dimers OW7–OW7′ [2.760(4) Å] and OW8–OW8′ [2.789(4) Å], where the primed atoms are generated by inversion. In this way, the structure most probably contains H-bonded pairs $[ClO_4–H–ClO_4]^-$ and $[HO–H–OH]^-$. It is worth noting that similar perchlorate dimers have been observed several times in various structures.[13]

Table 1. Selected bond lengths (Å) for **1** and **2**.

Yb^{3+}–EDTA			Yb^{3+}–CDTA		
Yb1–O5	2.238(2)	Yb1–O5	2.268(3)	Yb2–O24	2.277(3)
Yb1–O7	2.273(2)	Yb1–O7	2.273(2)	Yb2–O21	2.290(3)
Yb1–O3	2.228(2)	Yb1–O3	2.259(2)	Yb2–O25	2.252(3)
Yb1–O1	2.277(2)	Yb1–O1	2.273(2)	Yb2–O27	2.271(2)
Yb–O_{av}	2.254(25)	Yb1–O_{av}	2.268(7)	Yb2–O_{av}	2.273(16)
Yb1–OW1	2.320(2)	Yb1–OW3	2.313(3)	Yb2–OW4	2.349(3)
Yb1–OW2	2.323(3)	Yb1–OW1	2.305(3)	Yb2–OW2	2.299(3)
Yb–OW_{av}	2.322(2)	Yb1–OW_{av}	2.309(6)	Yb2–OW_{av}	2.324(35)
Yb1–N1	2.582(3)	Yb1–N1	2.555(3)	Yb2–N22	2.538(3)
Yb1–N2	2.572(2)	Yb1–N2	2.542(3)	Yb2–N21	2.560(3)
Yb–N_{av}	2.577(7)	Yb1–N_{av}	2.549(9)	Yb2–N_{av}	2.549(16)
Yb–Yb	7.329(3)	Yb–Yb	5.802(3)		

The other structure, Yb^{3+}–CDTA, contains two symmetry-independent $[Yb(CDTA)(H_2O)_2]^-$ anions, which have essentially the same geometry. The main difference between them consists in their neighbourhood. Namely, the anion containing Yb1 is involved in seven bonds to water molecules and in two hydrogen bonds to carboxylate oxygen atoms of adjacent complex anions, whereas the anion containing Yb2 is linked through six hydrogen bonds to water molecules and three to carboxylate O atoms. Apart from that, either anion forms six bonds to guanidinium cations. Both complex anions are mutually linked by a pair of hydrogen bonds (Figure 2).

Comparison between the present ytterbium structures and the previously reported Eu^{3+} complexes with ligands,[9b,10d,11,12] allows changes in the Ln^{3+} coordination sphere to be observed. The main discrepancy between the structures of the monomeric Eu^{3+} and Yb^{3+} complexes with EDTA, ensuing from the difference in the ionic radii of both ions, concerns different numbers of coordinated water molecules, that is, three in the case of Eu^{3+} and two for Yb^{3+}. In the case of the CDTA complexes, the coordination number of Eu^{3+} and Yb^{3+} is the same – 8. In contrast, the complex anions of Eu^{3+} form polymeric[12] or dimeric[11] units, whereas the anions of the Yb^{3+} complex are monomeric. The formation of H-bonded dimers, as described above, may be viewed, however, as the initial step of dimerization, not completed in the present case.

IR Spectra

The IR spectra of both ytterbium compounds as well as that of H_4EDTA and H_4CDTA were recorded in the range 50–4000 cm^{-1} (Figure 3). The broad and intense bands located in the spectral range between 2500 and 3750 cm^{-1} are attributed to ν_{OH}, ν_{NH_2}, ν_{CH_2} oscillations. The sharp peaks at 2944 and 2862 cm^{-1} (ν_{CH_2} oscillations) of **2** are more intense than those of **1** as a result of the presence of a cyclohexane ring in the CDTA ligand. For both compounds, strong bands for the guanidinium δ_{NH_2} vibrations were found in the region 1640–1720 cm^{-1}. The bands attributed to the ν_{sCOO} and ν_{asCOO} oscillations are located at the same wavenumbers in the spectra of both crystals, that is, 1615 and 1403 cm^{-1}, respectively. This is caused by very similar geometries of the carboxylate groups (the $C–O_{coord}$ and $C–O_{uncoord}$ bond lengths and the O–C–O angles) in the studied Yb^{3+} complexes (Table 2).

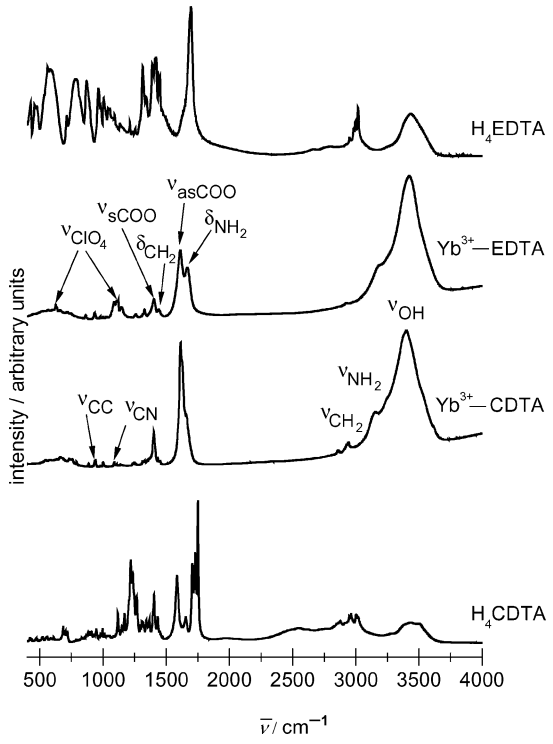

Figure 3. IR spectra of the Yb^{3+}–EDTA (**1**) and Yb^{3+}–CDTA (**2**) crystals and the respective ligands.

Table 2. Average C–O bonds length (Å) and angles (°) for crystals of **1** and **2**.

	Average bonds / Å		Average angles / °
	$C–O_{coord}$	$C–O_{uncoord}$	O–C–O
Yb^{3+}–EDTA (**1**)	1.236(6)	1.280(6)	124.2(5)
Yb^{3+}–CDTA (**2**)	1.240(2)	1.281(7)	124.8(7)

The ν_{CN} vibrations are located at ca. 1090, 1110 and 1140 cm^{-1}. Because the guanidinium cations are present in both crystals, it is difficult to distinguish between the ν_{CN} vibrations of the $[C(NH_2)_3]^+$ ions from those of the EDTA and CDTA ligands. Moreover, in the spectrum of the Yb^{3+}–EDTA complex, the bands at about 1100 cm^{-1} overlap with ν_{ClO} vibrations from the perchlorate anion.

The bands observed between 50 and 500 cm^{-1} can be ascribed mostly to low-energy Yb–ligand oscillations (δ_{OLnO}, δ_{NLnN}, ν_{LnO} and ν_{LnN}), as well as to lattice vibrations.

NIR Spectroscopy

It was shown recently[8e,14] that f–f transitions of lanthanide complexes with organic ligands in the NIR spectral region may overlap overtone bands of higher molecular vibrations and/or their combinations. To be sure that no overtone bands are present in the spectra of the $^2F_{7/2} \rightarrow {}^2F_{5/2}$ transition of both Yb^{3+} crystals, the spectrum of the Lu^{3+}–EDTA crystal, isomorphous with **1**, was recorded as well. The NIR spectra of the crystals are displayed in Figure 4. Because no weak peaks of $3\nu_{NH_2}$ and $3\nu_{OH}$ overtones were found in the lutetium spectrum, all peaks observed for **1** should be attributed to transition between the $^2F_{7/2}$ and $^2F_{5/2}$ multiplets.

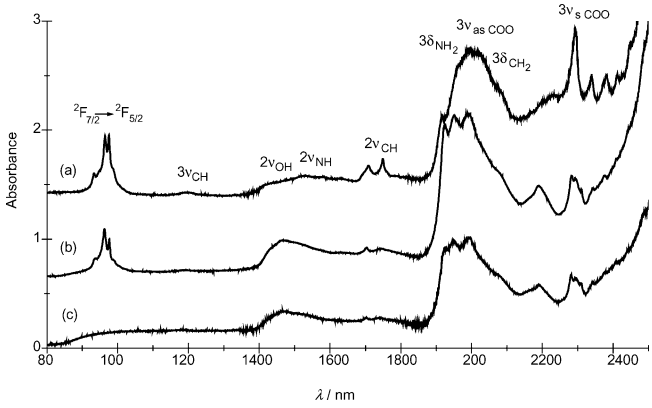

Figure 4. NIR spectra of (a) Yb^{3+}–CDTA (**2**), (b) Yb^{3+}–EDTA (**1**) and (c): Lu^{3+}–EDTA single crystals.

The spectra recorded at room temperature for the two crystal orientations (**a** and **b**) differ with respect to the observed intensity of the crystal field components, but not to their positions (Figure 5). Because the lines of the $^2F_{7/2}$ and $^2F_{5/2}$ manifolds are better resolved for the **b** orientation, the lower temperature spectra for this orientation are displayed in Figure 5, only. As it may be seen there, the electron–phonon coupling of the $^2F_{5/2}$ manifold is more pronounced in **1**. To perform a detailed analysis of the $^2F_{5/2}$ state in both crystals, the electronic (at 4.5 K) and IR (at 300 K) spectra were compared. This comparison is presented in Figure 6. Whereas the first two lines from the IR region of **1** are undoubtedly of electronic origin, the assignment of the third zero-phonon line, which should occur in the spectral range 10590–10720 cm^{-1}, is uncertain. Among three peaks located in the latter range, probably the middle one, for which the vibronic coupling with the first crystal-field

level is the weakest, may be attributed to a zero-phonon line. The two remaining peaks from this region must be then of vibronic origin. Contrary to **1**, the lowest-energy band in the spectrum of **2** is split into two sharp lines, which are 19 cm^{-1} apart. Their half widths, 16 cm^{-1}, are nearly the same as that of the lowest-energy zero-phonon line of the $^2F_{7/2} \rightarrow {}^2F_{5/2}$ transition in **1** (15 cm^{-1}). The doublet structure of this band is in accordance with the results obtained from the X-ray analysis, which proves that there are two Yb^{3+} sites in **2**. Because of the overlapping electronic lines coupled with vibrations of each Yb^{3+} ion, the remaining zero-phonon lines in **2** are broader than those in **1** and a vibronic structure of the $^2F_{7/2} \rightarrow {}^2F_{5/2}$ transition is also more blurred.

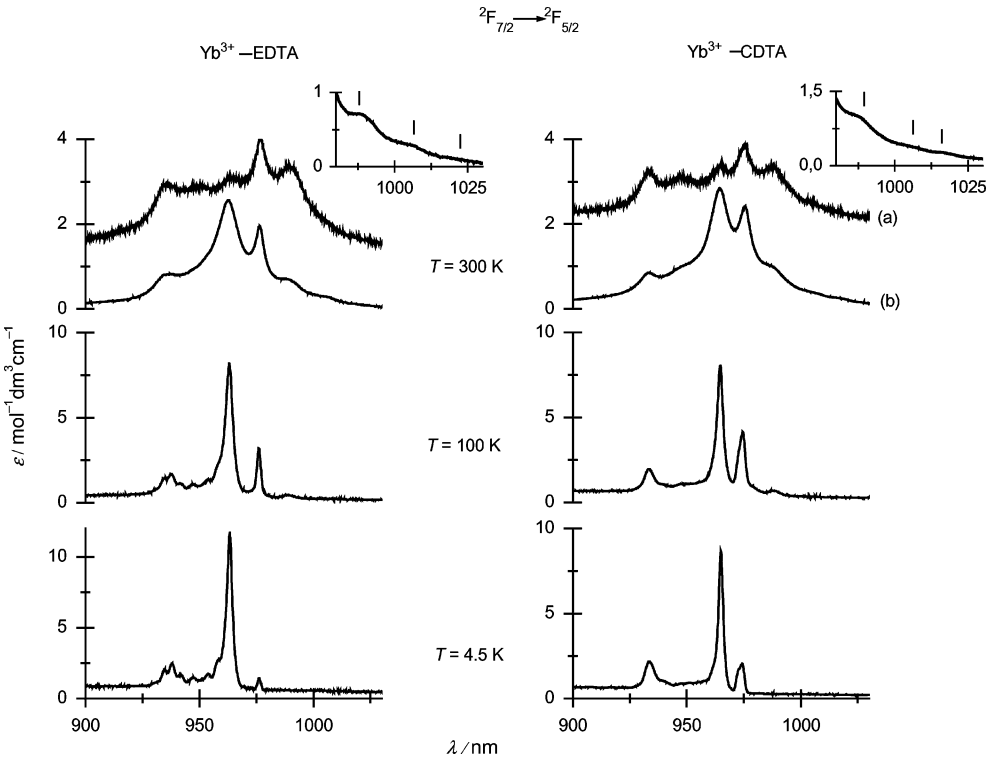

Figure 5. Absorption spectra of $^2F_{7/2} \rightarrow {}^2F_{5/2}$ transition for Yb^{3+}–EDTA and Yb^{3+}–CDTA crystals at different temperatures. The room-temperature spectra are drawn for both crystal orientations (**a** and **b**); for 100 and 4.5 K, only spectra taken for the **b** orientation are given. The inserts show hot components.

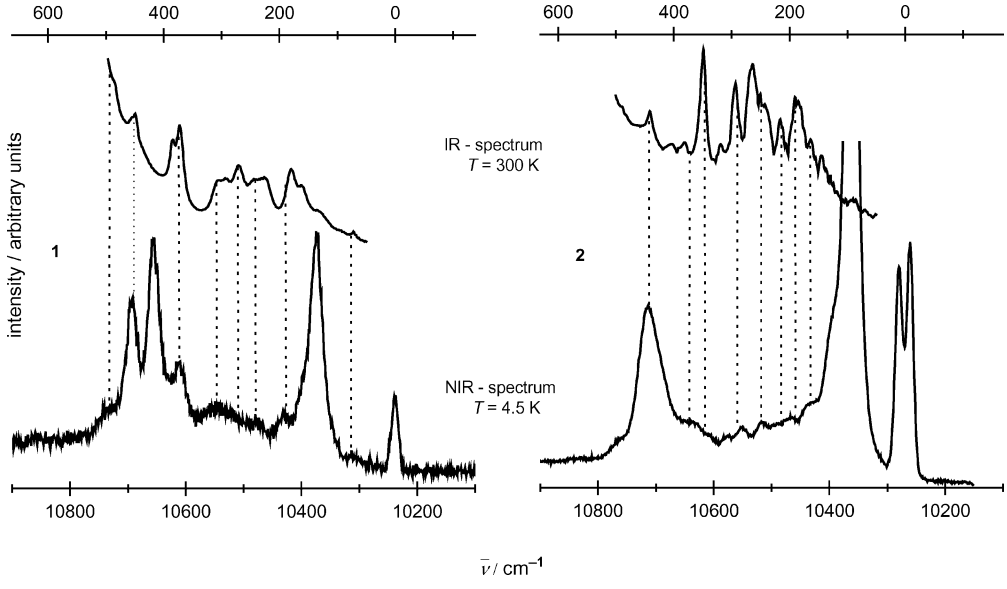

Figure 6. IR spectra (upper trace) and absorption $^2F_{7/2} \rightarrow {}^2F_{5/2}$ spectra recorded at 4.5 K (lower trace) of Yb^{3+}–EDTA (**1**) and Yb^{3+}–CDTA (**2**) compounds.

As all attempts to record the $^2F_{5/2} \rightarrow {}^2F_{7/2}$ emission spectra of both crystals through direct excitation into the $^2F_{5/2}$ state, as well in the UV region, failed, the energy-level diagram for the $^2F_{5/2}$ and $^2F_{7/2}$ states of the Yb^{3+} ion was proposed on the basis of absorption spectra only (Figure 7). Because the positions of the two highest levels of the $^2F_{7/2}$ ground state could not be confirmed from luminescence spectra, they are evaluated with some uncertainty, as it can be seen in the inserts in Figure 5. One may observe from diagrams given in Figure 7 that the position of the lowest level of the excited state is very sensitive to slight changes in coordination geometry around the Yb^{3+} ion. The inspection of the Yb–ligand distances given in Table 1 discloses that the energy of this level is strongly connected with the Yb–O (COO^-) distances, namely, their shortening is accompanied by lowering of the lowest $^2F_{5/2}$ crystal-field component. The presented results clearly reveal a high sensitivity of the $4f^{13}$ configuration on minor changes in coordination geometry around the Yb^{3+} ion.

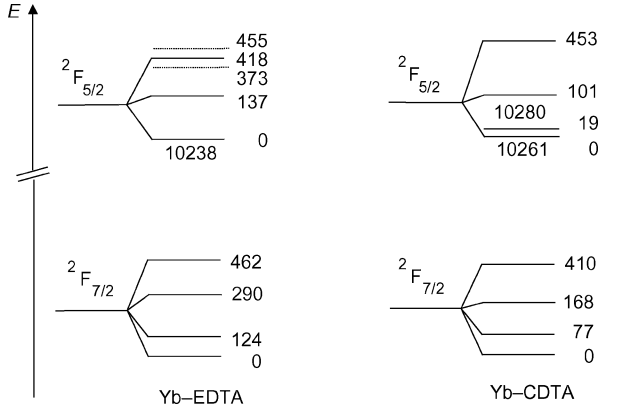

Figure 7. Energy-level diagrams for the Yb^{3+}–EDTA and Yb^{3+}–CDTA crystals.

The oscillator strength values (P) of the $^2F_{7/2} \rightarrow {}^2F_{5/2}$ transition were also determined from the spectra measured at 300 and 4.5 K of both crystals. The results are summarized in Table 3. The decrease in P by approximately 20% by lowering the temperature is mainly caused by depopulation of higher crystal-field levels of the $^2F_{7/2}$ term. In Table 3, the P values of related Yb^{3+} complexes in solution (obtained from dissolution of the respective crystals) are also given. Whereas the oscillator strength values of the Yb^{3+}–EDTA complex determined for the crystal and solution are nearly the same, the P value of the Yb^{3+}–CDTA complex in solution is higher than that in the crystal as well as those evaluated for the Yb^{3+}–EDTA system. It is worth noting that no differences between the spectra of the above solutions and those of solutions containing Na^+ as a countercation in the pH range 3.5–9.0 were observed.

The absorption spectra of Yb^{3+}–EDTA and Yb^{3+}–CDTA complexes in water solution are presented in Figure 8. For comparison purposes the averaged spectra of crystals (see Experimental Section) were also placed in this Figure. One may notice a high similarity between the spectra of the Yb^{3+}–EDTA complex in both phases, whereas

Table 3. Oscillator strength values (P) of Yb^{3+}–EDTA and Yb^{3+}–CDTA complexes in solutions and in crystals.

	Orientation	Yb^{3+}–EDTA		Yb^{3+}–CDTA	
		$P \times 10^8$			
		300 K	4.5 K	300 K	4.5 K
Crystal	**a**	395	210	325	314
	b	435	350	414	344
	average	**415**	276	**370**	329
Solution		**420**		**468**	

some differences involving the shapes and positions of peak maxima are well seen in the spectra of the Yb^{3+}–CDTA system. These results may indicate that geometries of complexes in both phases are similar in the case of Yb^{3+}–EDTA and differ for Yb^{3+}–CDTA. Our results do not allow us to decide unequivocally whether this difference is brought about by slow interchange between different conformers existing in solution and/or by a fluctuating number of coordinated water molecules. Different coordination behaviours of EDTA and CDTA towards Ln^{3+} ions in water solutions was also previously noticed by Graeppi et al.[15]

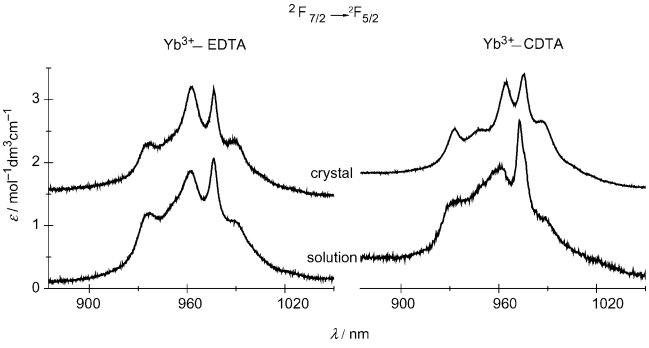

Figure 8. Spectra of $^2F_{7/2} \rightarrow {}^2F_{5/2}$ transition for Yb^{3+}–EDTA and Yb^{3+}–CDTA single crystals (averaged) and their solutions.

UV Spectroscopy

Absorption spectra in the UV range of Lu^{3+}–EDTA and Yb^{3+}–EDTA crystals are shown in Figure 9. The intense absorption begins at around 250 nm in the case of the lutetium compound owing to $\pi \rightarrow \pi^*$ transitions in the EDTA anion[16] and guanidinium cation,[17] whereas in **1** it starts earlier (at ca. 270 nm) due to the occurrence of the CT transition.[18] In order to isolate this band, the spectrum of **1** was recorded with respect to the reference Lu^{3+}–EDTA crystal. The Yb^{3+} and Lu^{3+} crystals were of the same thickness and orientation. To the best of the authors' knowledge, the band presented in Figure 9 is the first example of a charge-transfer transition isolated in an absorption spectrum of a Yb^{3+} molecular complex in the crystalline state. The CT transition of the Yb^{3+}–EDTA complex in solution was isolated in the same way. The half widths of these bands are 5700 and 6100 cm^{-1} for the crystal and solution, respectively. The estimated oscillator strengths of this transition are equal to 1×10^{-3} for the crystal and 3×10^{-3} for the solution. As the CT transitions are sensitive to molecu-

lar vibrations,[19] the three times higher oscillator strength in solution may be caused by molecular motions within the surroundings of the Yb^{3+} ion. Both these magnitudes are in the range found for the CT transitions in the Yb^{3+} systems in inorganic crystals[18,20] and in solutions.[21]

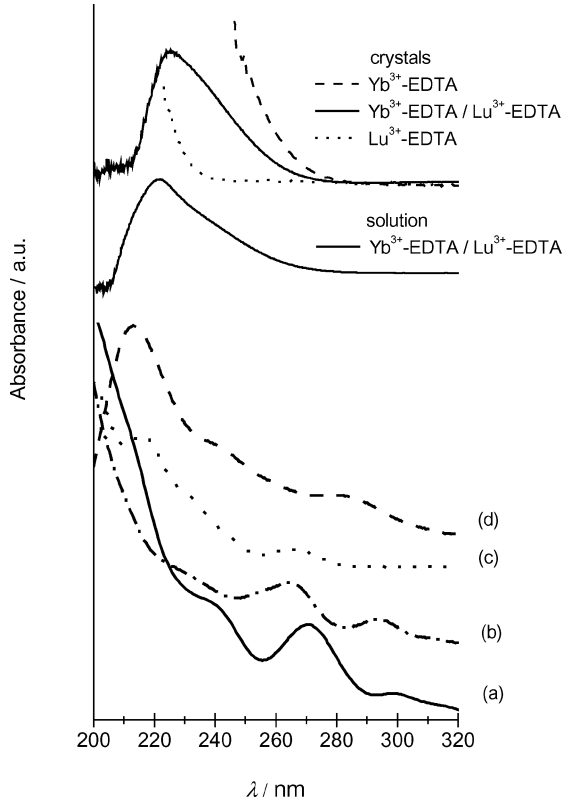

Figure 9. Experimental and simulated absorption curves related with the Yb^{3+}–EDTA system. The experimental curves are the following: Yb^{3+}–EDTA – absorption of **1**, Lu^{3+}–EDTA – absorption of $[C(NH_2)_3]_2[Lu(EDTA)(H_2O)_2]ClO_4{\cdot}6H_2O$, Yb^{3+}–EDTA/Lu^{3+}–EDTA – difference of the two former ones. For the theoretical curves the meaning of the symbols (a through d) of the simulated spectra is the same as in the Experimental Section (Theoretical Calculations).

As it was mentioned above, all attempts to excite (with UV and X-rays) an emission from the CT level in the present compound at room temperature and 77 K were unsuccessful. It was probably caused by efficient luminescence quenching brought about by energy transfer to different excited levels of the ligand and $[C(NH_2)_3]^+$ cation, which are located near the relevant excited levels of Yb^{3+}.

In order to elucidate the nature of the observed CT band, density functional theory calculations were performed for the $[Yb(EDTA)(H_2O)_2]^-$ anion, which allowed simulation of the electronic absorption spectra in the range 200–320 nm (Figure 9). Generally, the calculation results were function-basis-dependent, and the agreement between the experimental and observed spectra is rather qualitative; for that reason, a more-detailed discussion of the computational outcome would be premature. Nevertheless, some conclusions based of common features and trends observed for all sets of results may be reached. The experimental absorption in the Yb^{3+}–EDTA crystal starts at approximately 270 nm. This is roughly rendered in the simulated spectra, although the absorption onset structure is not in exact agreement with the experimental spectrum. Apart from the deficiency in the theoretical approach, this may be brought about by the absorption of the $[C(NH_2)_3]^+$ cations not included in the calculations. As previously noticed, the use of SAOP (model c–Experimental Section) causes shifting of the simulated bands towards shorter wavelengths.[22]

The electronic structure of the anion may be described as follows: In the HOMO region, the occupied 4f orbitals of Yb are interspersed with the nonbonding orbitals of the oxygen atoms from the carboxylate groups; for that reason, the obtained canonical orbitals were mixtures of both types. Nonetheless, the unpaired spin density was reproduced correctly as residing on the metal cation. Both the HOMO and LUMO are the 4f orbitals of Yb, but the highest occupied carboxylate orbital is only ca. 700 cm^{-1} below the HOMO. Above the LUMO there are two virtual orbitals (located at 24000–26000 and 28000–31000 cm^{-1} above the HOMO for the models with the PW91 functional and 36000 and 41000 cm^{-1} for SAOP) composed of the empty orbitals of water with a remarkable admixture of 6s and 7s (the lower) or 5d and 6d (the higher) functions of Yb. Above them, the virtual orbitals are mostly centred on the carboxylate groups, and the majority of them have smaller or larger admixtures of 6d and sometimes 5d functions of the metal. Accordingly, as far as the ytterbium cation is concerned, there seems to be three main types of excitations in the range of approximately 200–320 nm that contribute to the calculated absorption spectrum. The first group consists of transitions from π orbitals of the carboxylate groups to the empty 4f orbital of Yb (the L→Yb transitions). These transitions occur in the whole region of interest, but they are rather concentrated towards the lower energies of the considered region. Curiously enough, they contribute to a rather small extent to the calculated absorption spectrum. The second group (of the Yb→L type) is composed of the excitations from the 4f orbitals to the empty water levels, described above; they also occur at rather lower energies. The third set (also Yb→L), which constitutes the majority of the Yb and involves excitations below approximately 270 nm, consists of transitions from the 4f levels of Yb to empty orbitals in the carboxylate groups.

Thus, the calculations suggest that the CT transition in the present compound is dominated by excitations from the metal 4f orbitals to those of the ligands. This is a rather unexpected result and may be tentatively explained by high negative charge of the EDTA anion and concomitant high energy of the HOMO of the ligand.

Conclusions

New crystal structures of EDTA and CDTA complexes of Yb^{3+} were determined. In each crystal, the coordination sphere of the Yb^{3+} ion consists of four oxygen and two nitrogen atoms from the ligands and two water molecules (coordination numbers are 8). For the Yb^{3+} ion, the ligand-

field components of the ground $^2F_{7/2}$ and excited $^2F_{5/2}$ states were proposed. It was found that the components are sensitive to small alterations in the surroundings of the metal. The structural and spectroscopic data for these compounds in monocrystals and in solutions suggest that the coordination environments of the metal ion are similar in both phases in the case of the EDTA complex, whereas they are different for the Yb^{3+}–CDTA system. For the first time, the CT transition was located in the absorption spectrum of a crystalline complex of ytterbium with an organic ligand, and the theoretical calculations for this transition showed its complicated (Yb→L and L→Yb) character.

Experimental Section

Materials and Sample Preparation: Stock solutions of ytterbium chloride, ytterbium perchlorate and lutetium perchlorate were prepared by dissolving Yb_2O_3 (99.99%, Standford Materials) or Lu_2O_3 (99.9%, SERVA) in 2 M hydrochloric or perchloric acid, respectively. The metal concentration was determined complexometrically by using xylenol orange as an indicator. Equimolar quantities of ytterbium or lutetium perchlorate solution (6 mmol) and solid H_4EDTA (98%, MERCK; 6 mmol) were mixed together and heated at 90 °C (±5 °C) until precipitates dissolved. Next, solid $[C(NH_2)_3]_2CO_3$ (ABCR) was added to the solutions to adjust to pH 4. Large colourless crystals of $[C(NH_2)_3]_2[Yb(EDTA)(H_2O)_2]$-$ClO_4$·$6H_2O$ (**1**) and those of the isomorphous Lu^{3+} compound were formed after 3 d.

The crystals of $[C(NH_2)_3][Yb(CDTA)(H_2O)_2]$·$4H_2O$ (**2**) were prepared as follows: ytterbium chloride solution (3 mmol) and solid H_4CDTA (98%, Lancaster; 3 mmol) were heated at 90 °C (±5 °C). After dissolution of the substrates, the mixture was alkalized with $[C(NH_2)_3]_2CO_3$ to a final pH value of 3.5, and the solution was left for crystallization. Large colourless crystals of **2** were formed after ca. three months.

Solutions of Yb^{3+}–EDTA, Lu^{3+}–EDTA and Yb^{3+}–CDTA used for spectroscopic measurements were prepared by dissolving relevant amounts of appropriate crystals in water as well as by mixing $Ln(ClO_4)_3$ and ligand solutions in the molar ratio of 1:1.1. NaOH was added to adjust to a pH value in the range of 3.5 and 9.

Crystal Structure Determinations of Complexes 1 and 2: Suitable crystals were cut from larger ones, mounted on a Kuma KM4 diffractometer equipped with a CCD counter and measured at 100 K. The structures were solved routinely by using Patterson synthesis. The C- and N-bonded hydrogen atoms were placed in positions calculated from the geometry, and those bonded to O atoms were found from difference Fourier maps; not all were found. The final refinement was anisotropic for all non-H atoms. The computations were performed with the SHELXS97[23] and SHELXL97[24] programs, and the molecular graphic was prepared with DIAMOND.[25]

Crystal Data for 1: $C_{12}H_{40}ClN_8O_{20}Yb$, M = 825.01, triclinic, space group $P\bar{1}$, Z = 2, a = 11.067(7) Å, b = 11.153(6) Å, c = 13.033(7) Å, α = 90.60(5)°, β = 91.63(5)°, γ = 110.65(5)°, V = 1504.3(15) Å^3, μ = 3.29 mm^{-1}, $D_{calcd.}$ = 1.821 g cm^{-3}, $F(000)$ = 830, crystal size = 0.22 × 0.2 × 0.1 mm, h = 3–28.5°, index ranges: $-11 \le h \le 14$, $-14 \le k \le 14$, $-16 \le l \le 17$, reflections collected/unique = 10013/6527 (R_{int} = 0.0232). Final R indices for $I > 2\sigma(I)$: $R(F)$ = 0.0206, $R_w(F^2)$ = 0.0437 and for all data $R(F)$ = 0.0214, $R_w(F^2)$ = 0.0437, data completeness to 2θ = 56.6° 87.5%. Largest diff. peak and hole 0.893 and –0.521 e Å^{-3}.

Crystal Data for 2: $C_{15}H_{42}N_5O_{14}Yb$, M = 657.58, triclinic, space group $P\bar{1}$, Z = 2, a = 8.418(4) Å, b = 16.519(8) Å, c = 16.755(8) Å, α = 88.52(4)°, β = 83.35(4)°, γ = 83.39(4)°, V = 2298.7(19) Å^3, μ = 4.14 mm^{-1}, $D_{calcd.}$ = 1.900 g cm^{-3}, $F(000)$ = 1332, crystal size = 0.18 × 0.12 × 0.2 mm, h = 3–28.5°, index ranges: $-11 \le h \le 10$, $-21 \le k \le 20$, $-20 \le l \le 21$, reflections collected/unique = 15853/10040 (R_{int} = 0.0321). Final R indices for $I > 2\sigma(I)$: $R(F)$ = 0.0250, $R_w(F^2)$ = 0.0431 and for all data $R(F)$ = 0.0332, $R_w(F^2)$ = 0.0436, data completeness to 2θ = 56.6° 87.9%. Largest diff. peak and hole 1.422 and –0.821 e Å^{-3}.

CCDC-679552 (for **1**) and -679553 (for **2**) contain the supplementary crystallographic data for this paper. These data can be obtained free of charge from The Cambridge Crystallographic Data Centre via www.ccdc.cam.ac.uk/data_request/cif.

Spectroscopic Measurements and Calculations: IR spectra of the complexes in nujol suspensions and KBr pellets were measured in the range 50–4000 cm^{-1} with a Bruker FTIR IFS66 spectrometer. Electronic absorption spectra were recorded with a Cary 500 UV/Vis/NIR spectrophotometer. The spectra of crystals were measured at different temperatures (300–4.5 K) in a continuous flow helium cryostat (Optistat, Oxford), and the spectra of solutions were taken at room temperature. The room-temperature spectra of both crystals were measured at two different orientations (**a** and **b**) with respect to the light beam, and the averaged curves were then used for a comparison with the spectra of relevant solutions. The averaged curves were obtained from the relation outlined in Equation (1):

$$\varepsilon_{av} = \frac{\varepsilon_{\mathbf{a}} + \varepsilon_{\mathbf{b}}}{2} \quad (1)$$

where $\varepsilon_{\mathbf{a}}$, $\varepsilon_{\mathbf{b}}$ are molar absorption coefficients, as functions of λ, for the **a** and **b** orientations of the crystals, respectively.

The oscillator strengths (P) were determined by using equation (2):

$$P = \frac{4.32\times10^{-9}}{c\,d} \cdot \int_{\sigma_1}^{\sigma_2} A(\sigma)\,d\sigma \quad (2)$$

where c is the concentration of the Yb^{3+} ion in M, d is the length of the optical way in cm and $A(\sigma)$ is the absorbance as a function of the wavenumber in cm^{-1}.

Theoretical Calculations: The electronic structure of the $[Yb(EDTA)(H_2O)_2]^-$ anion was calculated by using the density functional approach with the ADF suite of programs.[26] In the first step, the geometrical structure was optimized to get the acceptable positions of the H atoms. In this step, the coordinates of Yb and all non-H atoms were frozen. The electron density functional used was Perdew–Wang exchange and correlation functional (PW91)[27] and the basis was TZ2P+ with the core frozen up to 4d for Yb, and DZP for the other atoms; the 1s functions were frozen for C, N and O. The scalar relativity was included by using the ZORA[28] method; the bases scaled to ZORA, supplied with the ADF packet, were used. The second step included freezing all the coordinates and computing the electronic structure of the complex anion together with simulating the spectra with the supplied time-dependent DFT.[29] The following settings were used: model a: PW91 with TZ2P+ frozen up to 4d for Yb and TZ2P for other atoms with 1s

frozen for C, N, O; model b: PW91 with TZ2P+ and DZP for Yb and other atoms, respectively; model c: SAOP with TZ2P+ for Yb and TZ2P for other atoms; model d: PW91 with QZ4P for all atoms.

The relativity treatment was described previously. There were serious problems with convergence, which were probably brought about in part by high obtained energies of occupied nonbonding orbitals of EDTA oxygen atoms, which had values very similar to those of the 4f orbitals of Yb. The other effect of such state was that the resulting canonical orbitals were usually mixtures of the 4f and the oxygen nonbonding orbitals.

Acknowledgments

Density functional calculations were carried out at the Wrocław Centre for Networking and Supercomputing (http://www.wcss.wroc.pl), grant No. 58.

[1] T. F. Gritmon, M. P. Goedken, G. R. Choppin, *J. Inorg. Nucl. Chem.* **1977**, *39*, 2021–2023.
[2] S. Aime, S. Geninatti Crich, E. Gianolio, G. B. Giovenzana, L. Tei, E. Terreno, *Coord. Chem. Rev.* **2006**, *250*, 1562–1579.
[3] a) I. Hemmilä, V. Laitala, *J. Fluoresc.* **2005**, *15*, 529–542; b) T. Nishioka, K. Fukui, K. Matsumoto in *Handbook on the Physics and Chemistry of Rare Earths* (Eds.: K. A. Gschneidner Jr., J.-C. G. Bünzli, V. K. Pecharsky), Elsevier, Amsterdam, **2007**, vol. 37, p. 174.
[4] J. A. Peters, J. Huskens, D. J. Raber, *Prog. Nucl. Magn. Reson. Spectrosc.* **1996**, *28*, 283–350.
[5] S. Comby, J.-C. G. Bünzli in *Handbook on the Physics and Chemistry of Rare Earths* (Eds.: K. A. Gschneidner Jr., J.-C. G. Bünzli, V. K. Pecharsky), Elsevier, Amsterdam, **2007**, vol. 37, p. 217.
[6] a) W. D. Horrocks Jr., J. P. Bolender, W. D. Smith, R. M. Supkowski, *J. Am. Chem. Soc.* **1997**, *119*, 5972–5973; b) R. M. Supkowski, J. P. Bolender, W. D. Smith, L. E. L. Reynolds, W. D. Horrocks Jr., *Coord. Chem. Rev.* **1999**, *185–186*, 307–319.
[7] W. T. Carnall, P. R. Fields, B. G. Wybourne, *J. Chem. Phys.* **1965**, *42*, 3797–3806.
[8] a) A. Mondry, P. Starynowicz, *Inorg. Chem.* **1997**, *36*, 1176–1180; b) A. Mondry, P. Starynowicz, *J. Chem. Soc., Dalton Trans.* **1998**, 859–863; c) A. Mondry, P. Starynowicz, *Polyhedron* **2000**, *19*, 771–777; d) A. Mondry, P. Starynowicz, *New J. Chem.* **2000**, *24*, 603–607; e) A. Mondry, P. Starynowicz, *Eur. J. Inorg. Chem.* **2006**, 1859–1867.
[9] a) J. Gałęzowska, R. Janicki, A. Mondry, R. Burgada, T. Bailly, M. Lecouvey, H. Kozłowski, *Dalton Trans.* **2006**, 4384–4394; b) A. Mondry, R. Janicki, *Dalton Trans.* **2006**, 4702–4710.
[10] a) B. Lee, M. D. Lind, J. L. Hoard, *J. Am. Chem. Soc.* **1965**, *87*, 1611–1612; b) J. L. Hoard, B. Lee, M. D. Lind, *J. Am. Chem. Soc.* **1965**, *87*, 1612–1613; c) L. R. Nassimbeni, M. R. W. Wright, J. C. van Niekerk, P. A. McCallum, *Acta Crystallogr., Sect. B* **1979**, *35*, 1341–1345; d) K. Nakamura, T. Kurisaki, H. Wakita, T. Yamaguchi, *Acta Crystallogr., Sect. C* **1995**, *51*, 1559–1563; e) N. Sakagami, J. I. Homma, T. Konno, K. I. Okamoto, *Acta Crystallogr., Sect. C* **1997**, *53*, 1376–1378; f) N. Sakagami, Y. Yamada, T. Konno, K. Okamoto, *Inorg. Chim. Acta* **1999**, *288*, 7–16.
[11] J.-G. Kang, S.-K. Yoon, Y. Sohn, J.-G. Kim, Y.-D. Kim, I.-H. Suh, *J. Chem. Soc., Dalton Trans.* **1999**, 1467–1473.
[12] R. Janicki, A. Mondry, P. Starynowicz, *Polyhedron* **2007**, *26*, 845–850.
[13] a) B. Graham, M. T. W. Hearn, P. C. Junk, C. M. Kepert, F. E. Mabbs, B. Moubaraki, K. S. Murray, L. Spiccia, *Inorg. Chem.* **2001**, *40*, 1536–1543; b) H. Oshio, M. Yamamoto, T. Ito, *Inorg. Chem.* **2002**, *41*, 5817–5820; c) L. Tei, M. Arca, M. C. Aragoni, A. Bencini, A. J. Blake, C. Caltagirone, F. A. Devillanova, P. Fornasari, A. Garau, F. Isaia, V. Lippolis, M. Schroder, S. J. Teat, B. Valtancoli, *Inorg. Chem.* **2003**, *42*, 8690–8701; d) D. Armentano, G. De Munno, R. Rossi, *New J. Chem.* **2006**, *30*, 13–17.
[14] a) A. Mondry, K. Bukietyńska, *Mol. Phys.* **2003**, *101*, 923–934; b) A. Mondry, K. Bukietyńska, *J. Alloys Compd.* **2004**, *374*, 27–31.
[15] N. Graeppi, D. H. Powell, G. Laurenczy, L. Zékány, A. E. Merbach, *Inorg. Chim. Acta* **1995**, *235*, 311–326.
[16] R. Janicki, A. Mondry, P. Starynowicz, *Z. Anorg. Allg. Chem.* **2005**, *631*, 2475–2477.
[17] R. J. Sension, B. Hudson, P. R. Callis, *J. Phys. Chem.* **1990**, *94*, 4015–4025.
[18] P. Dorenbos, *J. Phys. Condens. Matter.* **2003**, *15*, 8417–8434.
[19] J. C. Krupa, *J. Alloys Compd.* **1995**, *225*, 1–10.
[20] E. Nakazawa, *J. Lumin.* **2002**, *100*, 89–96.
[21] B. Keller, K. Bukietyńska, B. Jeżowska-Trzebiatowska, *Bull. Pol. Acad. Sci. Chem.* **1976**, *24*, 763–769.
[22] P. Starynowicz, *Dalton Trans.* **2007**, 2779–2783.
[23] G. M. Sheldrick, *SHELXS-97: Program for Structure Solution*, University of Göttingen, **1997**.
[24] G. M. Sheldrick, *SHELXL-97: Program for Structure Refinement*, University of Göttingen, **1997**.
[25] *DIAMOND-Visual Crystal Structure Information System*, CRYSTAL IMPACT, Postfach 1251, 53002 Bonn, Germany.
[26] a) G. te Velde, F. M. Bickelhaupt, E. J. Baerends, C. Fonseca Guerra, S. J. A. van Gisbergen, J. G. Snijders, T. Ziegler, *J. Comput. Chem.* **2001**, *22*, 931–967; b) C. Fonseca Guerra, J. G. Snijders, G. te Velde, E. J. Baerends, *Theor. Chem. Acc.* **1998**, *99*, 391–403; c) E. J. Baerends, J. Autschbach, A. Bèrces, C. Bo, P. M. Boerrigter, L. Cavallo, D. P. Chong, L. Deng, R. M. Dickson, D. E. Ellis, M. van Faassen, L. Fan, T. H. Fischer, C. Fonseca Guerra, S. J. A. van Gisbergen, J. A. Groeneveld, O. V. Gritsenko, M. Grüning, F. E. Harris, P. van den Hoek, H. Jacobsen, L. Jensen, G. van Kessel, F. Kootstra, E. van Lenthe, D. A. McCormack, A. Michalak, V. P. Osinga, S. Patchkovskii, P. H. T. Philipsen, D. Post, C. C. Pye, W. Ravenek, P. Ros, P. R. T. Schipper, G. Schreckenbach, J. G. Snijders, M. Solá, M. Swart, D. Swerhone, G. te Velde, P. Vernooijs, L. Versluis, O. Visser, F. Wang, E. van Wezenbeek, G. Wiesenekker, S. K. Wolff, T. K. Woo, A. L. Yakovlev, T. Ziegler, *ADF2005.01, SCM, Theoretical Chemistry*, Vrije Universiteit, Amsterdam, The Netherlands, http://www.scm.com.
[27] J. P. Perdew, J. A. Chevary, S. H. Vosko, K. A. Jackson, M. R. Pederson, D. J. Singh, C. Fiolhais, *Phys. Rev. B* **1992**, *46*, 6671–6687.
[28] a) E. van Lenthe, E. J. Baerends, J. G. Snijders, *J. Chem. Phys.* **1993**, *99*, 4597–4610; b) E. van Lenthe, E. J. Baerends, J. G. Snijders, *J. Chem. Phys.* **1994**, *101*, 9783–9792; c) E. van Lenthe, A. Ehlers, E. J. Baerends, *J. Chem. Phys.* **1999**, *110*, 8943–8953.
[29] a) S. J. A. van Gisbergen, J. G. Snijders, E. J. Baerends, *Comput. Phys. Commun.* **1999**, *118*, 119–138; b) A. Rosa, E. J. Baerends, S. J. A. van Gisbergen, E. van Lenthe, J. A. Groeneveld, J. G. Snijders, *J. Am. Chem. Soc.* **1999**, *121*, 10356–10365.

Received: March 10, 2008
Published Online: May 21, 2008

